WELDING RESEARCH

SUPPLEMENT TO THE *WELDING JOURNAL,* SEPTEMBER 2008
Sponsored by the American Welding Society and the Welding Research Council

Automatic Weld Planning by Finite Element Simulation and Iterative Learning

An automatic off-line planning system was developed to predict the optimum control variables in gas metal arc welding

BY P. V. JEBERG, H. HOLM, AND O. MADSEN

ABSTRACT. This paper presents a system for automatic planning of gas metal arc welding (GMAW) operations. The system automatically generates optimal dynamic trajectories of welding control variables (power input, current, and voltage; and travel speed) such that a desired weld quality is obtained despite known changes in process conditions, for example, geometric changes.

The system is based upon a finite element simulation of the GMAW process. The finite element model developed for the purpose consists of two parts: a heat conduction model simulating the temperature distribution within the workpiece and a model simulating the weld pool surface shape. To improve the accuracy of the finite element model, a calibration method has been developed that enables precise simulation with varying welding control variables.

The finite element simulation is coupled to an iterative learning controller, which exploits the capability of simulations to be repeated. The iterative learning controller identifies the best possible dynamic trajectories of the welding control variables in an iterative process.

The results of open loop execution of automatically planned GMA welding on butt joints with constant and varying thermal regions are presented. A comparison with industrially applied data showed that a significant reduction of the heat input and workpiece distortion could be achieved while maintaining a satisfactory weld quality. The results demonstrate the superiority of process performance based on planning by iterative learning control compared to manual execution of welding task and compared to process planning based on traditional methods.

*P. V. JEBERG (*peter.jeberg@disagroup.com*), a former employee of Department of Technology Development, Odense Steel Shipyard, Odense, Denmark, is now with DISA Industries, Herlev Hovedgade Denmark. H. HOLM* (i9hh@iprod.aau.dk) *and O. MADSEN* (i9om@iprod.aau.dk) *are with Department of Production, Aalborg University, Aalborg East, Denmark.*

Introduction

For many years, steel-structure fabrication companies have introduced welding robots in the effort to remain competitive. The robots are capable of improving the arc on time, removing humans from hazardous work environment, and securing a more homogeneous weld quality. To increase the productivity of welding robots, off-line programming is an often used method, but off-line programming has been confined to planning the robot motion. The welding control variables are set based on resource consuming welding experiments, and they are therefore not necessarily optimized with regard to heat input. Instead, the settings of the welding control variables are just usable settings, which result in an acceptable weld quality for the entire weld task. In general, constant values of the welding control variables entail that the variables are set in a conservative manner, such that the process is kept well within the usable process window. However, this can result in too large heat input and in too much added material compared to what will be possible with dynamic trajectories of the welding control variables, which are optimized with regard to minimum heat input. Too high heat input and too much added material have a negative effect on workpiece distortion and consequently on production efficiency. However, obtaining process optimized dynamic welding control variables by use of experiments is also costly, especially if the geometry complexity entails a change in thermal process conditions along the weld joint. This calls for a method for automatic and optimal planning of dynamic trajectories of the welding control variables.

KEYWORDS

Automatic Planning
Finite Element Model
Gas Metal Arc
Iterative Learning
Welding Variables

During the last decades arc welding has been simulated by numerical methods, especially by finite element methods. A comprehensive overview of finite element analysis and simulation of welding has been made by Mackerle (Ref. 1). However, only few references exist to work where numerical models have been used directly for automatic weld planning. Doumanidis (Refs. 2, 3) presents results of off-line planning of trajectories of the plasma arc heat source in scan welding. More recently, Ericsson (Ref. 4) presents a finite element based method to optimize the gas tungsten arc welding (GTAW) process.

This paper focuses on a system for automatic and optimized planning of the GMA welding operations. The system builds upon a concept for automatic weld process planning and online real-time feedback control created at Aalborg University, Denmark (Refs. 5–10). The struc-

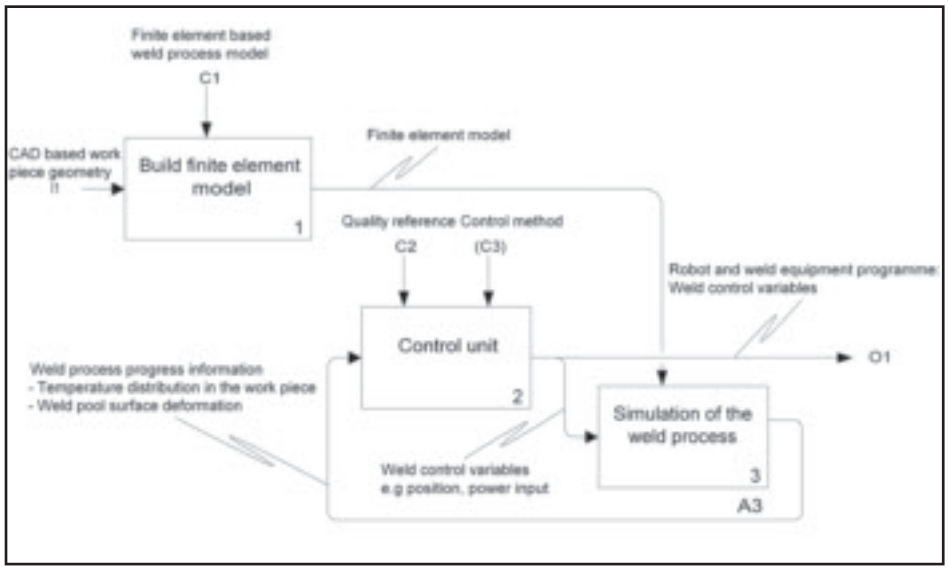

Fig. 1 — The off-line process-optimized weld planning system.

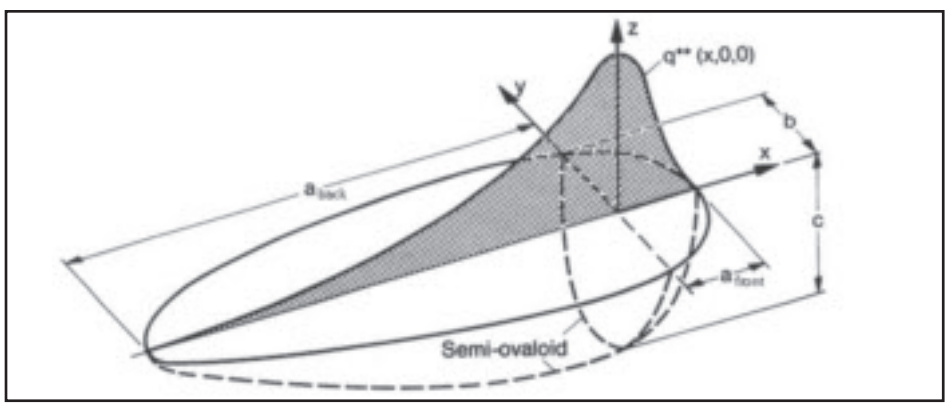

Fig. 2 — Volumetric heat source (Ref. 12).

ture of the system is presented along with the finite element model and the iterative learning algorithm used to perform the process optimization. At present, the system is used to plan butt joint complete penetration single-pass GMA-welding tasks. The results of open-loop execution of planned weld tasks are presented. A more thorough description of the system can be found in Ref. 8.

Off-Line Process Optimized Weld Planning

The automatic off-line planning system consists of two parts. One part is the finite element model, which models the workpiece geometry and the welding process. The other part of the planning system is a control function, which is used to optimize the simulated process. Figure 1 shows a diagram of the off-line process-optimized weld planning system. During simulation, the weld process information is sampled at each time step to identify the weld process progress. Depending on the control method, the information can either be used to adjust the values of the process control variables for the next time step, or the information can be saved and used to update the entire trajectory of the process control variables before a new simulation is performed. The latter is the case with iterative learning control.

The control unit in Fig. 1 takes a quality reference as input, which as an example can be the maximum allowed weld pool surface deformation or the minimum required size of the fusion zone. Based on the comparison of the quality reference and the process progress, the control unit makes rectifying actions on the values of the welding control variables such that the error between the desired quality and the process progress is minimized. In this way the controlled simulation identifies the optimal trajectories of the welding control variables with regard to the desired quality reference. The level of optimality depends on the effectiveness of the control method applied. A primary benefit of using a simulation in search of optimal settings of the welding control variables is removal of costly experiments in search of the optimal settings.

The trajectory of the optimized control variables is saved and used as a basis for a robot program used for the physical execution of the simulated weld task. If the agreement between the simulation and the physical world is good, the physical execution of the planned weld will result in an optimized process with regard to the quality reference. However, if the difference between the simulated and the physical world is not sufficiently small, a real-time feedback control system is needed. A real-time feedback control system based on a temperature-sensitive camera has been developed and presented in Ref. 9. The system compares the weld pool surface temperature profile obtained during execution with the reference weld pool surface temperature profile obtained during simulations. Hence, the off-line process-optimized planning system generates the real-time quality reference.

Finite Element Model

The finite element model for simulating complete joint penetration welding consists of two parts: a heat conduction model to simulate the temperature distribution within the workpieces and a weld pool surface shape model, which simulates the shape of the weld pool surface. The latter is of special interest when simulating complete joint penetration welding and welding on an inclined workpiece because in these cases there is an increased risk of breaking the weld pool surface. The two models are coupled together through the cross-sectional area of the weld pool. The location of the melting isotherm is identified by the heat conduction model, and is set to 1530°C (Ref. 8). The material within the area between the melting isotherms is considered to consist of liquid metal, and the domain of this area is transferred to the weld pool surface shape model as the domain of interest. Further description of the coupling of the models is presented in Refs. 8 and 10.

Heat Conduction Model

The heat conduction model calculates the heat distribution inside the workpiece

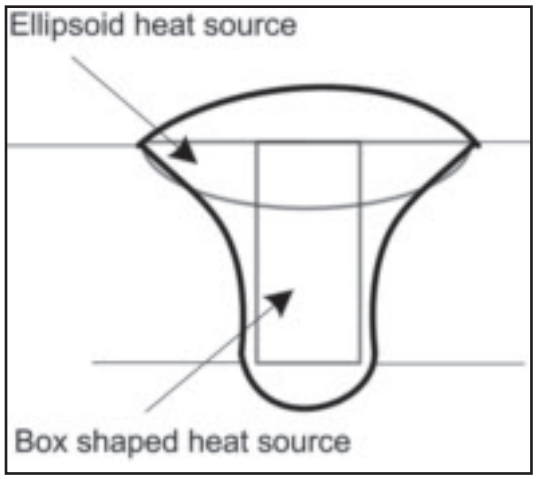

Fig. 3 — Sketch of the heat sources' area of action (gray lines).

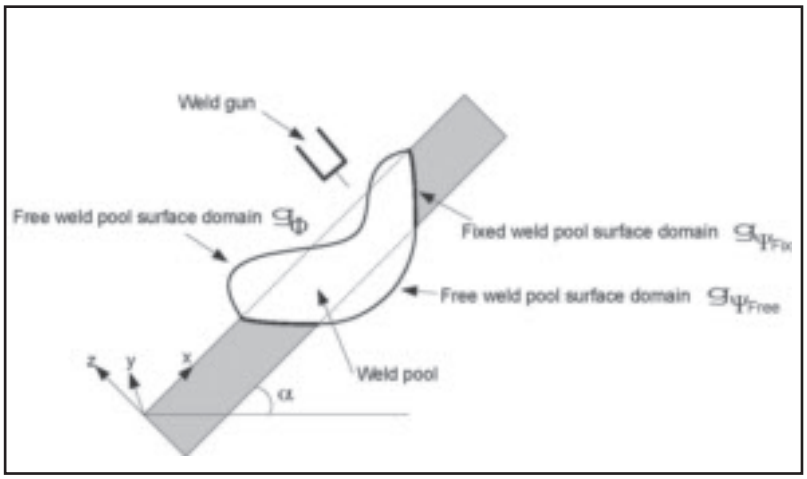

Fig. 4 — Model of workpiece and weld pool.

by use of Fourier's heat conduction equation. On the surface, the heat transport is determined by convection and radiation (Ref. 11). The use of Fourier's heat conduction equation is based on constant values for density of metal (ρ), convection and radiation factors, temperature-dependent values of thermal conductivity (*k*),and heat capacity (*c*) (Ref. 8).

The power input to the workpiece from the welding arc and liquid metal is simulated by two different heat sources, which are following each other along the weld joint. The first heat source is a three-dimensional volumetric heat source (Ref. 12):

$$Q_v'''\left(x^*,y^*,z^*\right) = \frac{6\sqrt{3}fQ_{\mathit{eff}}}{abc\pi\sqrt{\pi}} e^{-\left(\frac{3x^{*2}}{a^2}+\frac{3y^{*2}}{b^2}+\frac{3z^{*2}}{c^2}\right)} \quad (1)$$

Q_v''' represents the power input to the workpiece [W/m^3], x*,y*,z* represent space coordinates relative to the position of the heat source, and Q_{eff} represents the effective power delivered by the ellipsoid heat source. *a,b,c* represent variables that control the energy distribution within the workpieces. *a* is divided into two parts a_{front} and a_{back} used in front of and behind the heat source center. *f* represents a factor used to change the energy induced into the workpiece in front of and behind the heat source center. f_{front} and f_{back} is calculated based on a continuous heat source distribution across the x = 0 plan (Ref. 12). With the volumetric heat source, it is possible to approximate the weld pool tail and to obtain a rounded shape of penetration. A drawing of the area of action of the volumetric heat source can be seen in Fig. 2.

The second heat source is a box-shaped heat source (Ref. 8). This heat source was introduced because of material addition, which represents an abrupt transition from an empty joint to a joint filled with liquid metal. The domain Ω_{box} of the box-shaped heat source is the width of the joint, the workpiece thickness, and the length moved by the heat source in each time step during simulation. The power Q_{box} is equally distributed inside the box

$$Q_v'''\left(x,y,z\right) = \begin{cases} \dfrac{Q_{box}}{V_{box}}\left(x,y,z\right) \in \Omega_{box} \\ 0 \quad \left(x,y,z\right) \notin \Omega_{box} \end{cases} \quad (2)$$

Here, V_{box} represents the volume of the box-shaped heat source domain. A cross-section drawing of the two heat sources' area of action can be seen in Fig. 3.

The total heat input *Q* to the workpiece is calculated based on the heat input from the power supply (Voltage *U* · Current *I*) and the efficiency (η): $Q = U \cdot I \cdot \eta$. The total heat input *Q* is distributed to the workpiece in two ways by the two heat sources: as Q_{eff} by the three-dimensional volumetric heat source and as Q_{box} by the box-shaped heat source. The two contributions fulfill the constraint $Q = Q_{\mathit{eff}} + Q_{box}$. During all experiments, both for calibration and the subsequent validation, the voltage *U* and current *I* are chosen such that a usable and stable welding process is obtained. The relationship between *U* and *I* is determined during initial experiments. The relation between *U* and *I* is also used when planning the process-optimized welding task, where the relation is used to determine the *U* and *I* settings based on the value of heat input *Q*, which is identified as giving the optimal process.

It is important to remember that the heat conduction model does not include any fluid properties of the liquid metal in the weld pool. The heat sources are instead used to simulate the effect of energy distribution caused by the convection of liquid metal.

Weld Pool Surface Shape Model

The weld pool surface shape model (Fig. 4) is used to calculate the surface deformation in the z-direction (vertically to the workpiece surface).

The domain for the weld pool surface shape model is identified by an approximation of the melting point isothermal in the heat conduction model (Ref. 10). The surfaces of the weld pool will in a static equilibrium attain a deformation configuration, which results in minimum energy contents. Based on this energy consideration and the mathematical method of Calculus of Variation, the following deformation equations were developed (Refs. 8 and 13):

$$\begin{aligned} &P_a\left(x,y\right) + \rho g \sin\left(\alpha\right)\bullet x + \rho g \cos\left(\alpha\right) \\ &\bullet\Phi - \lambda - \nabla\left(\frac{\gamma\nabla\Phi}{\sqrt{1+\left|\nabla\Phi\right|^2}}\right) = 0 \\ &-\rho g \sin\left(\alpha\right)\bullet x - \rho g \cos\left(\alpha\right) \\ &\bullet\left(\Psi - s\right) + \lambda - \nabla\left(\frac{\gamma\nabla\Psi}{\sqrt{1+\left|\nabla\Psi\right|^2}}\right) = 0 \end{aligned} \quad (3)$$

In the above equation, $P_a(x,y)$ is the arc pressure, ρ is the density of liquid metal and is considered as constant (Ref. 8), *g* is gravity and is constant, α is the workpiece

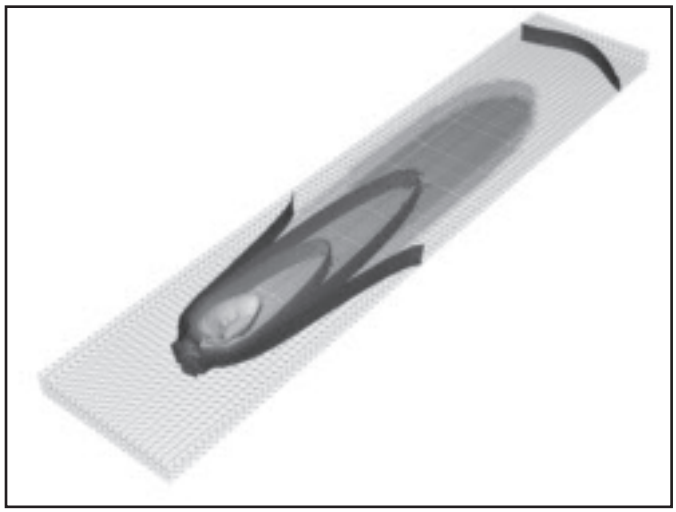

Fig. 5 — Temperature distribution in the heat conduction domain. The isotherms are set at 700°, 900°, 1100°, and 1530°C.

Fig. 6 — Fusion of the workpieces is shown by removing all elements that have been above the melting point. It shows that a complete joint penetration weld is obtained except from the start of welding. At the end of the welding, the weld pool gets wider because the heat input is not able to be conducted away from the fusion zone.

inclination, Φ and Ψ are the surface deformations of the uppermost and lowermost surfaces respectively, γ is the surface tension, *s* is the workpiece thickness, and λ is a La Grange multiplier, which connects the two equations, for example, by a constraint on the weld pool volume, or in this case of GMA welding, a constraint on the cross section of the crown. The distribution of the arc pressure $P_a(x,y)$ is calculated by an exponential equation (Equation 4), which is a practical simplification of a physically description of $P_a(x,y)$ (Ref. 14).

$$P_a\left(x,y\right)=P_{a,\max}\bullet e^{\frac{x^2+y^2}{\kappa}} \quad (4)$$

In GMAW, the continuous feed wire adds material to the welding process, which is used for filling up the joint. Excessive material forms a crown of material on the surfaces of the workpieces, while observing the mass constraint present in Equation 5.

$$\dot{V}_{crown}=\dot{V}_{wire}-\dot{V}_{gap} \quad (5)$$

$\dot{V}_{crown}$, $\dot{V}_{wire}$, and $\dot{V}_{gap}$ are the rate of material used for the crown, rate of filler metal added, and rate of material used to fill the joint. The material used on the crown in the simulation is obtained by identifying the outermost deformation contour of the weld pool surface. This is expected to be equal to the final shape of the crown. This can be formulated as:

$$\dot{V}^*_{crown}\left(\lambda\right)=v\bullet\int\Phi_{contour}\left(y,\lambda\right)-\Psi_{contour}\left(y,\lambda\right)dy \quad (6)$$

$\dot{V}^*_{crown}$ is the simulated rate of material used on the crown, *v* is the welding speed, $\Phi_{contour}(y,\lambda)$, and $\Psi_{contour}(y,\lambda)$ are the outermost deformation contour of the weld pool surfaces at a given y-position (perpendicular to the welding direction). The constraint that should be fulfilled in search for the correct value of λ is then (Refs. 8 and 13)

$$\dot{V}_{crown}-\dot{V}^*_{crown}\left(\lambda\right)=0 \quad (7)$$

Each time the weld pool deformation is calculated, the following iterative calculation is performed: First, on the basis of an initial guess of λ, Equation 3 is solved. Second, the volume constraint is evaluated using Equations 5–7. Based on the results of the volume constraint, the value of λ is updated, and the process is repeated until an acceptable value of λ is obtained (Ref. 15).

Simulation Plots

Results from a simulation can be viewed in Figs. 5–8. The workpiece is 100 mm long, 40 mm wide, and 3 mm thick. Figure 5 shows the temperature distribution in the heat conduction domain by use of four isotherms: 700°, 900°, 1100°, and 1530°C. The last is the melting point of the metal and, therefore, the 1530°C isotherm identifies the boundary of the weld pool. Note that the picture also reveals the adaptive grid used. The fusion of the workpiece and the penetration can be identified in Fig. 6, which shows a reference grid containing the maximum temperatures obtained during simulation. All the elements in the grid, which have had temperatures above the melting point, are removed. It can be seen that complete joint penetration does not occur initially. Therefore, the energy input needs to be higher in the beginning to obtain complete joint penetration from the start of welding. It can also be seen that at the end of the welding process, the weld pool is getting wider in the bottom before the heat source is turned off. This is because the energy cannot be conducted away from the fusion zone at the end of the workpiece. This increases the risk of breaking the weld pool surface. To avoid this, the heat input should be reduced close to the end of the welding process.

Figures 7 and 8 show the surface deformation. Figure 7 shows the front surface deformation Φ_{top}. The center of the heat source is located at the origin of the coordinate system. The effect of the arc pressure can be seen as a depression on the surface. Figure 8 shows the back surface deformation Φ_{bottom}.

The simulation results indicate that the finite element model works. However, the simulation results are not usable for process prediction before the heat source and material addition functions are calibrated.

Calibration of Finite Element Model

Before the finite element based GMAW model can be used for weld planning, several model parameters need to be calibrated. Calibration is needed because the model includes several variables,

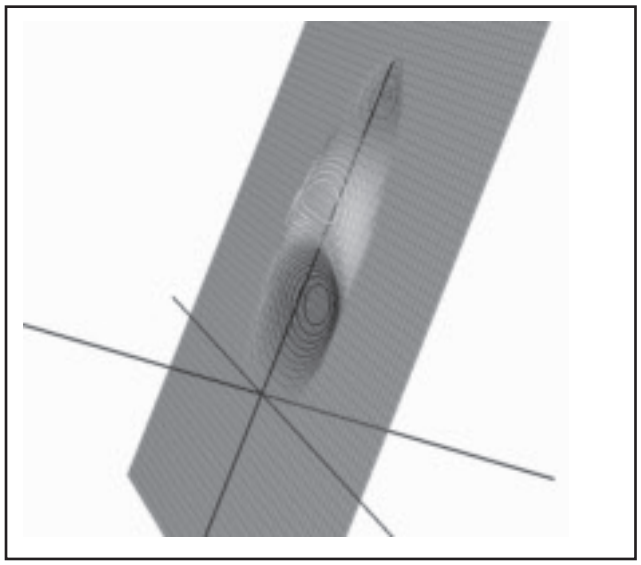

Fig. 7 — The top surface deformation Φ_{top} for the front surface. The heat source is moving from the top and down. The center of the heat source is located at the origin of the coordinate system.

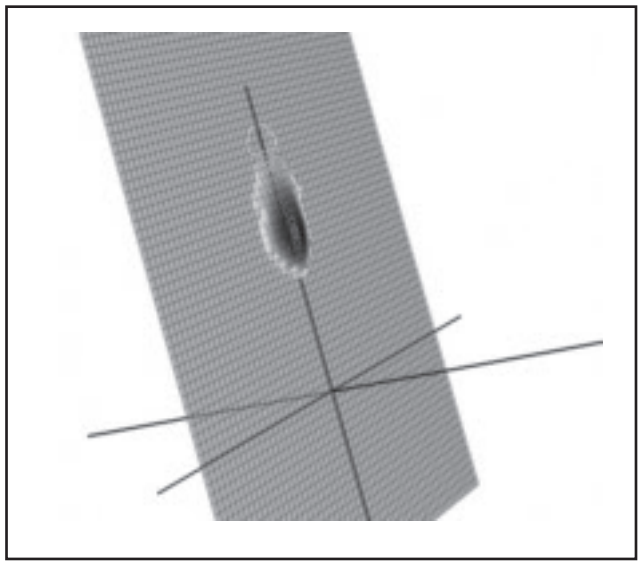

Fig. 8 — The bottom surface deformation Φ_{bottom} for the back surface. The heat source is moving from the top and down. The center of the heat source is located at the origin of the coordinate system.

which do not have any direct physical meaning. An example is the extension parameters *a, b* and *c* in the volumetric heat source. These parameters arise from describing physical properties by simplified expressions. Calibration can also be needed for parameters that have a physical meaning but for which it is difficult to obtain correct values. The developed GMAW model includes parameters of this type, e.g., surface tension γ. Surface tension varies with the actual composition of the material in the weld pool, e.g., the contents of sulfur.

The model parameters to calibrate in finite element model are

1) η, Q_{box} to calculate the power input to the workpiece and the distribution between the two heat sources in the heat conduction model.

2. a_{front}, *a, b, c* to calculate the shape of the three-dimensional volumetric heat source.

3. $P_{a,max}$, κ, γ to calculate the weld pool surface deformation.

The calibration of model parameters can be a complicated task to do manually because of the often nonlinear complex relation between parameter values and the simulated output. This makes the trial-and-error method unfeasible in practice. An automated optimization routine can therefore be helpful in search for the best parameter settings. In this research, an optimization routine called CFSQP (C code for feasible sequential programming, Ref. 16) is used together with the finite element software Diffpack (Ref. 17), which is a scientific-computing environment with emphasis on the finite element method. Overview of the integration can be seen in Fig. 9.

The calibration of a GMAW model can be performed in two different ways: either calibrate to a single experiment or calibrate to multiple experiments. Using a single experiment entails the parameter values to be constant when the model is used for prediction. When using multiple experiments, it is possible to identify the dependence of the model parameters with regard to changes in the control variables welding speed *v* and power input *Q*, and hence enable an interpolation of the parameter values throughout the process window when the model is used for prediction. In that way calibration to single or multiple experiments can have a large effect on the range of the acceptable prediction capability of the model. This can influence the usability of the calibrated model in search of optimal settings of the weld process control variables, hence the usability of the calibrated model in process optimized weld planning.

The welding process used for calibration is a top-down complete joint penetration, single-pass butt joint model calibrated to a 5-mm thick workpiece with a 2-mm weld joint width (Ref. 18). An overview of the experiments performed can be seen in Fig. 10. The multiple experiment calibration is performed in this research based on four experiments: QHWL, QLWL, QHWH, and QLWH. The remaining five points are used for validation of the obtained prediction

Table 1 — Results from Manual Welding of a Rectangular Workpiece

Current *I*(A)	194	Avg. weld speed *v*(mm/s)	5.33
Voltage *U*(V)	23	Heat Input *E*(kJ/mm)	0.84
ξ_{top} (mm)	7.1	ϕ_{top} (mm)	1.1
ξ_{bottom}(mm)	3.5	ϕ_{bottom}(mm)	1.3

Table 2 — Results from a Simulation and Optimization of Welding of a Rectangular Workpiece

Current *I*(A)	164	Avg. Weld speed *v*(mm/s)	5.68
Voltage U(V)	20	Heat Input *E*(kJ/mm)	0.58
ξ_{top} (mm)	7.4	ϕ_{top} (mm)	0.7
ξ_{bottom}(mm)	3.2	ϕ_{bottom}(mm)	1.5

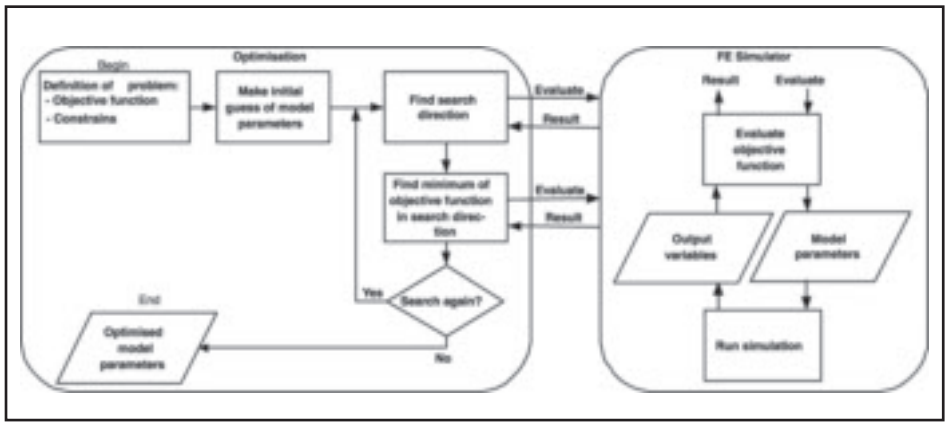

Fig. 9 — A diagram of the integration of the optimization routine and the finite element simulator.

Table 3 — Results from Two Welding Experiments on Rectangular Workpieces Using Optimized Variable

Ex. 1	Current I(A)	168	Avg. Weld speed	5.67
	Voltage U(V)	20.4	Heat Input E(kj/mm)	0.60
	ξ_{top} (mm)	5.9	ϕ_{top} (mm)	0.7
	ξ_{bottom}(mm)	3.3	ϕ_{bottom}(mm)	1.1
Ex. 2	Current I(A)	158	Avg. Weld speed	5.67
	Voltage U(V)	20.2	Heat Input E(kj/mm)	0.56
	ξ_{top} (mm)	4.9	ϕ_{top} (mm)	0.6
	ξ_{bottom}(mm)	3.0	ϕ_{bottom}(mm)	0.6

capability.

Test results from the validation of the model calibrated to a single experiment show a general increasing error level from the calibration experiment to the validation experiments. The results from validation of the model calibrated to multiple experiments do not show the same overall increasing error level. Figure 11 shows a picture of a polished cross section for validation point QMWL. Further elaboration of the calibration results can be found in Refs. 8 and 18.

The multiple experiments calibrated model does also succeed in identifying the process boundary. The three process boundary test experiments are outside the process window. Simulation of these experiments did predict a loss of weld pool. This indicates that the prediction capability of the multiple experiments calibrated model can be extrapolated outside the range of the calibration experiments. In addition to this, the model can be used to identify an approximate location of the process boundary beyond which the process will be invalid. This is an important property of the multiple experiments calibrated model, and it increases the usability of the model for weld planning.

When performing prediction of the welding process, the varying interpolated parameter values are identified by using a two-dimensional bilinear interpolation method, which is expected to be sufficient for obtaining a suitable model prediction capability. This two-dimensional bilinear interpolation method utilizes the multiple experiment calibration performed in this research, which is based on four experiments. To secure linear interpolation despite the location of the four experiment points in the process window, an isoparametric formulation of the two-dimensional bilinear interpolation method is introduced (Ref. 19), which is an essential formulation in the finite element method. The derivation and solving procedure can be found in Refs. 8 and 20.

In general, the gain of new knowledge, obtained from models, about the part of the process windows in which the models themselves have been trained or calibrated, can be questioned. This is because the same gain of knowledge might be retrieved from the experiments themselves without use of models. Interpolating model parameters is a method to improve the gain of knowledge and thereby the usefulness of models. The reason is that the density of necessary calibration points in the process window may be much lower than the density of necessary experimental points to obtain applicable process knowledge, e.g., to build a process database. The fewer necessary calibration points, the more useful the model is and less experimental resource consuming.

Iterative Learning Control

Iterative learning control (ILC) is a method for improving the transient response in an iterative process. Information about the output error e_k from iteration k is used to update the input u_{k+1} for the next iteration $k+1$. The basic principle can be seen in Fig. 12 where $u_k(t)$ is the input to, and $y_k(t)$ is the output from, the *k'th* process iteration at time t. The variables $y_d(t)$ and $u_{k+1}(t)$ are the desired output and input to the next process iteration, respectively.

Iterative learning control needs the following conditions to function (Ref. 22):

1) The initial conditions are identical in each iteration.

2) The disturbance is identical in each iteration.

3) The plant parameters are stationary or slowly varying.

4) Each iteration has the same duration.

5) The desired output y_d is identical in each iteration.

The use of ILC in the off-line process optimized weld planning system benefits from the fact that the simulation can be repeated an infinite number of times with zero disturbance, identical model parameters, and identical initial conditions. Normally, ILC is applied to processes where the input is a function of time. In welding applications, the input as a function of position along the weld joint x is of interest and therefore time t is replaced with distance x — Fig. 13. Each process iteration will have the same weld joint length and the five conditions for ILC to function are fulfilled.

The ILC algorithm used in the weld planning in this paper is

$$\bar{e}_k(n) = \bar{y}_d(n) - \bar{y}_k(n)$$

$$\bar{u}_{k+1}(n) = \bar{u}_k(n) + \bar{\bar{\zeta}} \bullet \bar{\bar{\Gamma}} \bullet \bar{E}_k(n) \bullet \bar{\bar{L}} \qquad (8)$$

where $\bar{u}_k(n)$, $\bar{y}_k(n)$, $\bar{y}_d(n)$, $\bar{e}_k(n)$ are the i-dimensional input vector, the j-dimensional output, desired output and error vectors at point, n respectively. The (i,i) dimensional diagonal damping matrix $\bar{\bar{\zeta}}$ is used to avoid oscillations in $\bar{u}_k$. The elements in $\bar{\bar{\zeta}}$ are in this paper set to the same value ζ. $\bar{\bar{\Gamma}}$ is the

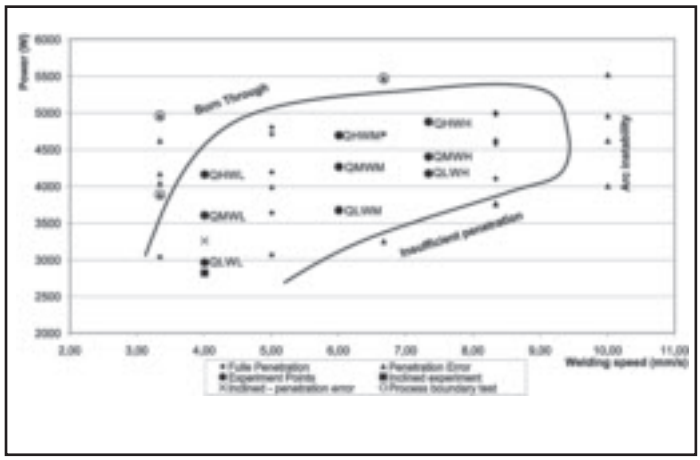

Fig. 10 — Diagram of the identified process window. The diamond and triangle show the experiment points in the first series of initial experiments. The triangles with a circle around are used to validate the capability of identifying the process boundaries. The round dots show the experiment points in the second series of experiments used for calibration and validation. The points are marked as Q and W for power and welding speed and L, M, and H for low, middle, and high level, respectively. The thick black curve shows the contour of the approximate process window.

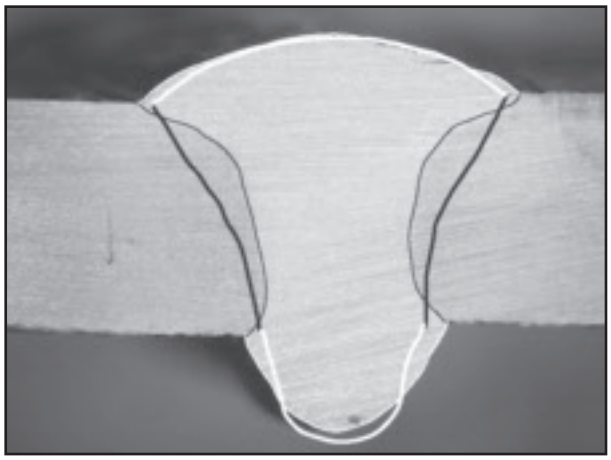

Fig. 11 — Picture of polished cross section for the validation point QMWL. The thin line marks the weld pool boundary, while the thick line marks the simulated weld pool boundary.

($\underline{i}$,j) dimensional error-weight matrix. $\bar{\bar{E}}_k(n)$ is the (j,m) dimensional error matrix, which includes the error vectors at different points n used to update $\bar{u}_k$. As an example $\bar{\bar{E}}_k(n)=[\bar{e}_k(n)\bar{e}_k(n+1)]$ where $m = 2$. $\bar{L}$ is the m-dimensional point-weight vector, which weights the influence of the error at different points n. n is the location on the workpiece along the weld joint — Fig. 13.

The error $e(n)$ is minimized with regard to the l_2-norm

$$\min\left\|\sqrt{\sum_{n=1}^{N}\bar{e}_{k,1}^2(n)}+\ldots+\bar{e}_{k,j}^2(n)\right\| \qquad (9)$$

Many different configurations of the ILC algorithm presented in Equation 8 are possible, which can have vital influence on the effectiveness and efficiency of the ILC method. Based on simulation tests, the following basic settings have been chosen (Ref. 23):

$$\bar{L}=\begin{bmatrix}0.6 & 0.4\end{bmatrix}^T,\zeta=25\%,\bar{\bar{E}}_k(n)=\left[\bar{e}_k(n)\ \ \bar{e}_k(n+1)\right]$$

and a 4-mm spacing between the points along the workpiece.

Simulation with Varying Workpiece Geometry

Simulation based on the heat conduction model is performed to illustrate the capability of process optimized weld planning with dynamic welding control variables. A sketch of the workpiece can be seen in Fig. 14.

The input is welding speed v and power input Q. The output is the widths of the fusion zone at the top ξ_{top} and the bottom ξ_{bottom} of the workpiece and hence $i = j = 2$. This gives the following input and error vector:

$$\bar{u}_k(n)=\begin{bmatrix}v_k(n) & \mathrm{Q}_k(n)\end{bmatrix}^T\ \bar{e}_k(n)$$
$$=\begin{bmatrix}e_{k,\xi_{top}}(n) & e_{k,\xi_{bottom}}(n)\end{bmatrix}^T \qquad (10)$$

The $\bar{\bar{\Gamma}}$ can be seen in Equation 11. Its values are based on information obtained during calibration of the model (Ref. 8). These settings entail that a too small ξ_{top} decreases v, and a too small ξ_{bottom} increases Q.

$$\bar{\bar{\Gamma}}=\begin{bmatrix}-1.1 & 0\\ 0 & 4.5e5\end{bmatrix} \qquad (11)$$

In Fig. 15 a comparison of the process optimized planned trajectory of the welding control variables with the initial constant-valued guess can be seen. The resulting width of the fusion zone of the initial guess and of the process optimized planned trajectory can be seen in Fig. 16.

The fusion zone width has primarily been optimized with regard to the bottom fusion zone width, which initially was too small compared to the desired reference. The process optimized trajectories of the control variables show as expected a significant variation in the welding speed v in the area where the workpiece width is small. The variation in power input Q in the area of the small workpiece width is not that significant, but it does show an increase.

The identified trajectories of the process control variables seen in Fig. 15 show settings, which are known to be outside the process window and will result in loss of the weld pool. In the ILC-based process optimization, only process progress information about the width of the fusion zone is used to update the input. As long as the error is not zero, the ILC method will continue to search along the direction given by $\bar{\bar{\Gamma}}$ although it crosses the process boundary and the weld pool is lost. Therefore, process progress information about the weld pool deformation will be included in weld planning for physical execution to identify when the process boundary is being crossed and the weld pool is lost.

Experiment with Rectangular Workpiece

To evaluate the benefit of the system for process optimized off-line weld planning at its present development status, two open loop execution experiments of planned optimized welding tasks were performed. The goal of the process optimized weld planning was to minimize the heat input while securing a minimum fusion zone width ξ_{min}, and a maximum crown height Φ_{max}. Φ_{max} was set in accordance with the welding standard used at Odense Steel Shipyard, which is 1.0 mm + 0.2·ξ. It is based on the standard DS/EN25817. However, the constraint on $\Phi_{max,\,bottom}$ was tightened by 0.5 mm in the optimization due to a model weakness.

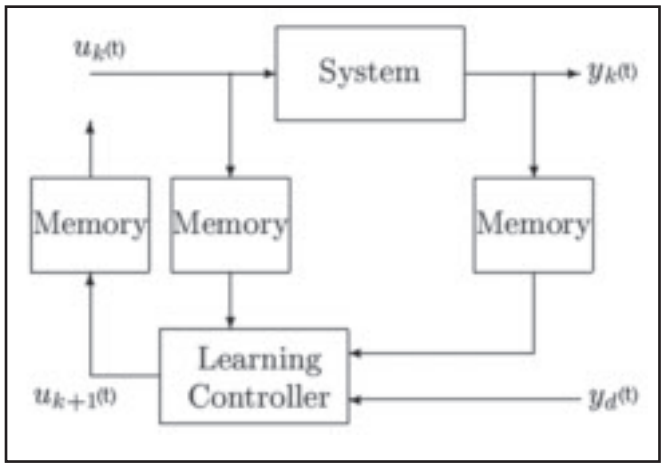

Fig. 12 — Diagram of the basic principle of ILC (Ref. 21).

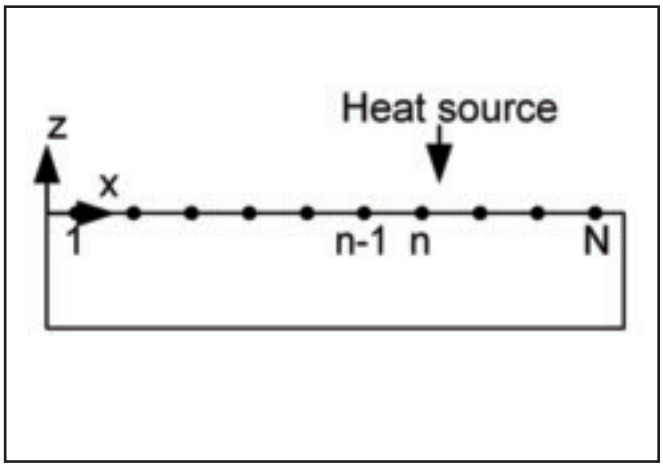

Fig. 13 — Sketch of the workpiece along the weld joint where the points 1..n..N are marked.

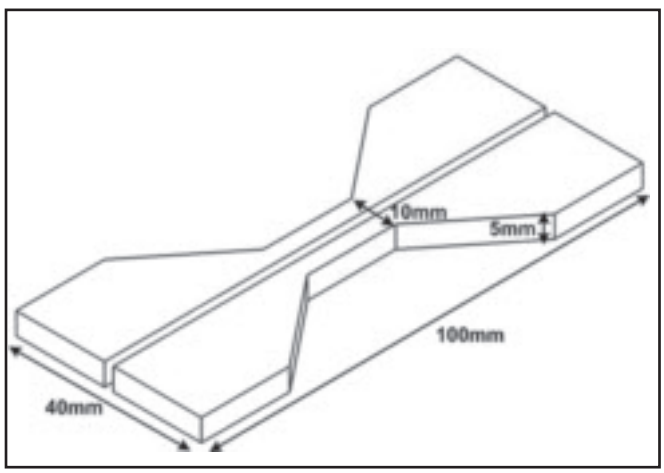

Fig. 14 — Picture of the nonuniform workpiece used for simulation.

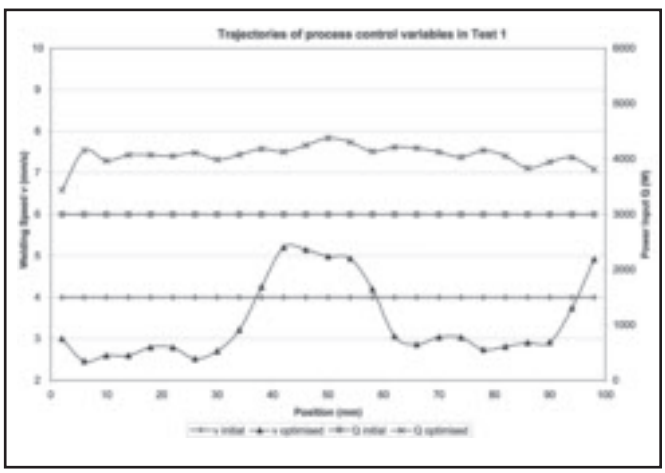

Fig. 15 — Graph of the process optimized planned trajectory of the welding control variables and the initial constant-valued guess.

Table 4 — Results from Manual Welding of a Nonuniform Workpiece

Process Settings	$I(A)$ 189	$U(V)$ 22.9	v(mm/s) 5.33	E(kJ/mm) 0.81
Pos.	ξ_{top}	ξ_{bottom}	ϕ_{top}	ϕ_{bottom}
40 mm	8.2 mm	3.4 mm	1.2 mm	1.5 mm
100 mm	12 mm	5.2 mm	1.9 mm	1.0 mm
160 mm	8.6 mm	3.7 mm	1.3 mm	1.1 mm

Table 5 — Results from Welding a Nonuniform Workpiece with Optimized Process Variables

Process Settings	$I(A)$ 177	$U(V)$ 20.9	v(mm/s) 5.50	E(kJ/mm) 0.67
Pos.	ξ_{top}	ξ_{bottom}	ϕ_{top}	ϕ_{bottom}
40 mm	6.6 mm	3.0 mm	1.3 mm	0.8 mm
100 mm	8.0 mm	3.7 mm	0.8 mm	0.9 mm
160 mm	6.9 mm	3.2 mm	0.9 mm	1.2 mm

This weakness is caused by the finite element model's lack of capability to fully simulate the outward opening of the weld pool at the bottom of the workpiece. This causes the model to predict a too small weld pool width at the bottom and hence a too small bottom crown height (Ref. 18). The constraint settings were

$\xi_{min,top} = 4.0$ mm

$\Phi_{max,\ top} = 1.0\text{ mm} + 0.2\cdot\xi_{top}$

$\xi_{min,bottom} = 3.0$ mm

$\Phi_{max,\ bottom} = 0.5\text{ mm} + 0.2\cdot\xi_{bottom}$

If the constraints are passed, the error will be different from zero and is included in the updating algorithm of $\tilde{u}_{k+1}$. In process optimized weld planning with regard to minimum heat input, the $\tilde{e}_k(n)$ and $\bar{\bar{\Gamma}}$ used can be seen in Equation 12A, which again is obtained from Ref. 8.

$$\bar{\bar{\Gamma}} = \begin{bmatrix} -1.1 & 0 & 0 & 0.58 & -1e\text{-}9 \\ 0 & 4.5e5 & 0 & 5e5 & 1.5e\text{-}4 \end{bmatrix} \quad (12A)$$

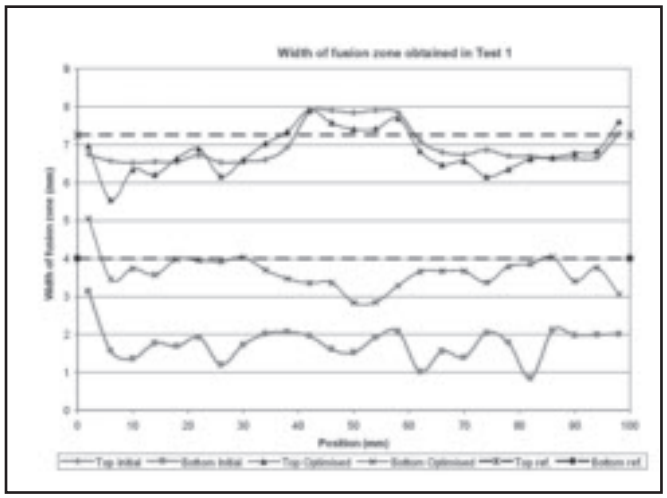

Fig. 16 — Graph of the resulting width of the fusion zone of the initial guess and of the process optimized planned trajectory. The desired reference is also shown.

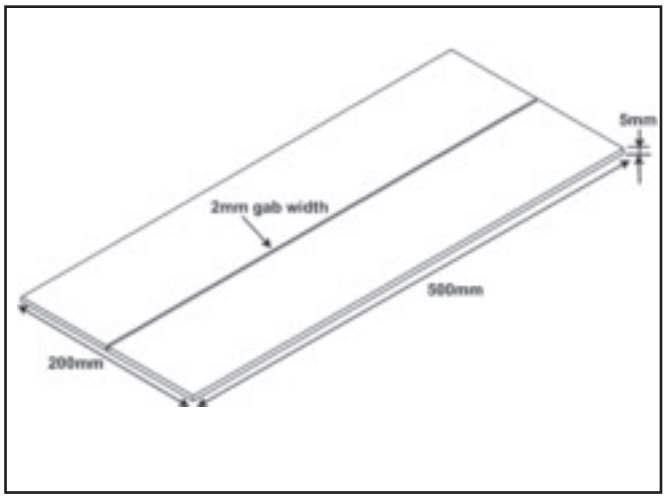

Fig. 17 — Picture of the rectangular workpiece used in the first open-loop experiment.

$$\bar{e}_k(n) = \begin{bmatrix} e_{k,\xi top}(n) e_{k,\xi bottom}(n) e_{k,\Phi top}(n) \\ e_{k,\Phi bottom}(n) e_{k,heat\ input}(n) \end{bmatrix}^T \quad (12B)$$

The first experiment was welding of a rectangular workpiece (Fig. 17), where the open-loop execution of a process optimized planned trajectory is compared with a manually executed weld.

The average settings of the process variable obtained during manual welding and the average resulting process output are shown in Table 1.

The result of the manual welding does in general fulfill the constraints except for Φ_{bottom}. However, Φ_{bottom} does not pass the welding standard used at Odense Steel Shipyard, except occasionally due to a variation caused by manual execution of the weld.

The manually obtained setting of the process variables was used as an initial guess for the process optimized weld planning. The planned process optimized trajectories of the process control variables reduced the relative error to 67%. The heat input E was reduced to 69% of that manually obtained. The planned process optimized trajectories showed minor fluctuations around an average value. The average values of the process control variables and the resulting simulated process output are shown in Table 2.

Again, the process output fulfilled the constraints except for Φ_{bottom}, which passed the constraint used during optimization by 0.4 mm, but the welding standard used at Odense Steel Shipyard was not passed.

Based on the heat input minimized weld planning, two open-loop executions (Ex. 1 and Ex. 2) were performed. The average values of the realized process control variables and the resulting process output are shown in Table 3.

The resulting process output of Ex. 1 was in most agreement with the planned weld. However, of major interest was the reduction in heat input to 71% and 67% for Ex. 1 and Ex. 2, respectively, compared to manual welding. The goal of the process optimized weld planning was to reduce heat input while the quality constraints were fulfilled. The reduction in heat input entailed a reduction in the deformation. The maximum deformation of the workpiece plate from its initial position was Manual ≈ 9 mm, Ex. 1 ≈ 4 mm, Ex. 2 ≈ 0 mm.

The deformation of Ex. 1 was reduced to 44% of the deformation obtained with manual welding, and the deformation of Ex. 2 was practically zero. This showed one of the benefits of using process optimized planned trajectories of the weld process control variables as mentioned in the introduction.

Experiment with Varying Workpiece Geometry

To investigate the effect of the process optimization with regard to minimizing heat input on a workpiece where the geometry changes influence on the thermal process conditions, a second experiment was performed. The workpiece, for which the trajectories of the optimal process control variables were planned, can be seen in Fig. 18.

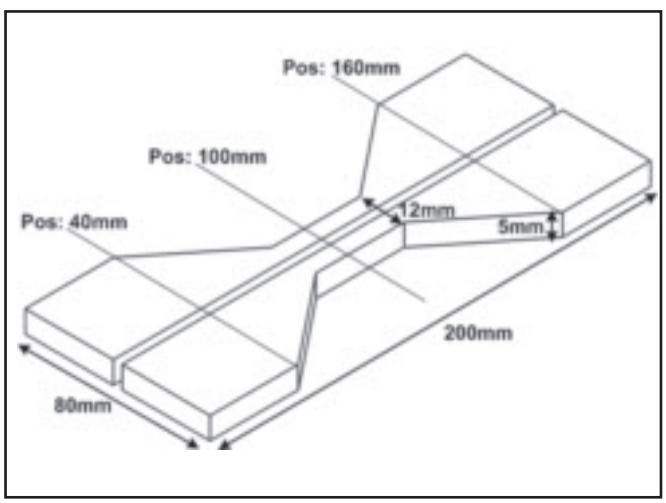

Fig. 18 — Picture of the nonuniform workpiece used in the experiment with a varying thermal region.

For comparison, the weld was executed using a robot and the manual settings of the process variables found in the experiment with the rectangular workpiece (Table 4). This gave results measured along the weld joint. The data fulfilled the demands from the welding standard:

In the narrow part of the workpiece, the weld pool was as wide as the workpiece, and examination of the workpiece showed that the edges were melted and the shape was altered.

The planned process optimized trajectories of the process control variables weld

speed v and power input Q were almost constant along the weld joint. This is because the quality constraints on the minimum fusion zone width ξ_{min} and the maximum crown height Φ_{max} were in general not violated during the optimization. When quality constraints on the minimum fusion zone width ξ_{min} and the maximum crown height Φ_{max} are not violated, the error $e_{k,\xi top}(n)e_{k,\xi bottom}(n)e_{k,\Phi top}(n)\ e_{k,\Phi bottom}(n)$ in Equation 12B is zero. This means that the result from the weld pool surface shape model is not included in calculating the error $e(n)$, which is minimized during the optimization. Instead the minimization of the error, and hence the update of the welding control variable, was predominated by the wish to minimize the heat input, which means that the optimization was based on results from the heat conduction model. This will cause a uniform update of the welding control variables when the initial guess is uniform. A more fine-tuned ILC based process optimized weld planning, which drives the process more to the edge of the process window, is expected to result in nonconstant process control variables as seen in Fig. 15, because the quality constraints are then expected to be activated. The improvement of the routine for ILC based process optimized weld planning is part of further work needed.

The planned weld was executed in an open loop and the obtained average values of the process control variables and the resulting process output are shown in Table 5.

The resulting process did also comply with the welding standard, and the heat input was minimized to 81% by using the process optimized settings. This reduction avoided melting of the workpiece edges, and it indicates how the weld planning system is able to handle changes in the process conditions.

Conclusion

A system for process optimized weld planning based on numerical simulation of the weld process by finite element, and iterative learning is presented. The system's present capability to perform weld planning that minimizes the heat input and hence workpiece distortion was tested. The results of welding width optimized welding control variables are promising.

The calibration of the GMA model to multiple points has shown a promising capability to predict the weld pool and surface shape within the process window. Going beyond the part of the process window in which the model is calibrated, the model has proven capable of identifying the process boundary between lost and not lost weld pool. This increases the model's usability in industrial applications when there is a search for optimal process settings, because optimal process settings can be rather robust and easy be located near the process boundary.

The capability of the weld planning system to obtain dynamic trajectories of the process control variables was shown in simulations of the welding of a workpiece with varying geometry. Especially, the welding speed showed clear variations. This is important in the planning of welds with varying material distribution around the weld joint, such as with pipe connections. The simulations also showed that not only information about the fusion zone width, but also information about the crown height are essential to reliable weld planning.

Acknowledgments

Odense Steel Shipyard Ltd. and the Danish Academy of Technical Science are acknowledged for the financial support, which made this research project possible.

References

1. Mackerle, J. 2002. Finite element analysis and simulation of welding — an addendum: a biography (1996–2001).

2. Doumanidis, C. C. 1995. Thermally optimal design by simulation of scanned materials processing methods. *Proceedings of the IASTED International Conference on Applied Modelling, Simulation and Optimization*, pp. 145–148.

3. Doumanidis, C. C. 1998. Thermal modelling and adaptive control of scan welding. *Welding Journal* 77(11): 465–475.

4. Ericsson, M. 2006. Simulation of robot paths and heat effects in welding. PhD thesis, Lund University and University West, Sweden, ISBN: 91-628-6869-1.

5. Holm, H., Kjeldsen, H. C. E., and Kristensen, J. K. 2003. A reference architecture for design of an industrial temperature feedback welding control system. *Journal of Materials Processing Technology* Vol. 139(1–3): 499–504.

6. Holm, H., Jeberg, P. V., and Bro, C. 2002. Application of numerical model for off-line programming of posture robot welding. *Proceedings of 12th International TWI Computer Technology in Welding and Manufacturing Conference*. Paper No. 81.

7. Terp, C. B., Holm, H., Høyer, J. H., and Nielsen, H. H. 1999. Welding process control based on a numerical model and state-space techniques. *Proceedings of the 18th IASTED International Conference Modelling, Identification and Control*, pp. 265–268.

8. Jeberg, P. V. 2005. Automatic process optimized weld planning of full penetration I-joint GMA welding. PhD thesis, Department of Production, Aalborg University, Denmark. ISBN: 87-91200-49-0.

9. Kjeldsen, H. C. 2006. Sensor based welding automation modelling system. PhD thesis, Department of Production, Aalborg University, Denmark.

10. Jeberg, P. V., Cai, X., Holm, H., and Langtangen, H. P. 2003. A flexible architecture for welding simulators used in weld planning. *Proceedings of International Conference on Productive Welding in Industrial Applications*, Lappenranta, Finland.

11. Mills, A. F. 1995. *Heat and Mass Transfer*. Irwin, 1st edition.

12. Goldak, J., Chakravarti, A., and Bibby, M. 1984. A new finite element model for welding heat source. *Metallurgical Transactions B* Vol. 15B(2): 299–305.

13. Jeberg, P. V., and Holm, H. 2003. 2D weld pool surface model in 3D space with one degree of freedom and its theoretical limitations for weld planning. *Proceedings of International Conference on Productive Welding in Industrial Applications,* Lappenranta, Finland.

14. Cao, Z. N., and Dong, P. 1998. Modelling of GMA weld pools with consideration of droplet impact. *Journal of Engineering Materials and Technology*, Transactions of the ASME, Vol. 120(4): 313–320.

15. Cai, X., Jeberg, P. V., and Langtangen, H. P. 2005. A numerical method for computing the profile of weld pool surfaces. *International Journal for Computational Methods in Engineering Science and Mechanics* 6(2): 115–125.

16. Lawrence, C. T., Zhou, J. L., and Tits, A. L. 1997. *User's Guide for CFSQP Version 2.5: A C Code for Solving (Large Scale) Constrained Nonlinear (Minimax) Optimization Problems, Generating Iterates*, TR-94-16r1, Institute for Systems Research, University of Maryland, College Park, Md.

17. Langtangen, H. P. 2003. *Computational Partial Differential Equations — Numerical Methods and Diffpack Programming*, 2nd edition, Springer Verlag.

18. Jeberg, P. V., and Holm, H. 2004. Simulation of full penetration GMA I-joint welding and identification of area of acceptable model performance. *Proceedings of 14th TWI International Conference on Computer Technology in Welding and Manufacturing*.

19. Cook, R. D., Malkus, D. S., and Plesha, M. E. 1989. *Concepts and Applications of Finite Element Analysis*, 3rd edition, John Wiley and Sons.

20. Jeberg, P. V., Holm, H., and Terp, C. B. 2004. Method for calibration of full penetration GMA I-joint welding model to single and multiple experiments. *Proceedings of 14th TWI International Conference on Computer Technology in Welding and Manufacturing.*

21. Moore, K. L. 1998. Iterative learning control — an expository overview. *Applied and Computation Controls, Signal Processing and Circuits*.

22. Pandit, M., and Baque, S. 1997. Learning control of cyclic production processes. *Proceedings of IEEE 6th International Conference on Emerging Technologies and Factory Automation*. pp. 64–70.

23. Jeberg, P. V., Holm, H., and Lambæk, S. 2005. Planning of dynamic trajectories for weld control variables by finite element simulation and iterative learning. *Proceeding of 7th International Conference on Trends in Welding Research,* Pine Mountain, Ga., ASM International, pp. 641–646.